Patterning-controlled morphology of spatially and dimensionally constrained oxide nanostructures

Zixiao Pan and Shuyou Li
Department of Materials Science and Engineering, International Institute for Nanotechnology, Northwestern University, Evanston, Illinois 60208, USA

Zhaoyu Wang and Min-Feng Yu
Department of Mechanical and Industrial Engineering, University of Illinois at Urban-Champaign, Urbana, Illinois 61801, USA

Vinayak P. Dravid[a)]
Department of Materials Science and Engineering, International Institute for Nanotechnology, Northwestern University, Evanston, Illinois 60208, USA

(Received 16 July 2007; accepted 9 September 2007; published online 1 October 2007)

This letter reports a facile approach for morphologic control of complex oxide nanostructures patterned by "soft" electron beam lithography (soft-*e*BL). The authors demonstrate fabrication of epitaxial nanofrustum and nanopyramidal morphologies of ferroelectric $BaTiO_3$ and magnetic $CoFe_2O_4$ lines, with controlled zig-zag or smooth edges. The dimensional and shape control is achieved by simply tuning the patterning parameters such as resist thickness and patterning directions with respect to underlying substrate orientation. The crystal orientation, element distribution, and piezoelectric behavior of $BaTiO_3$ nanofrustums are evaluated with analytical transmission electron microscopy and piezoresponse force microscopy. It is argued that soft-*e*BL allows for exquisite control over morphology, shape evolution, and orientation of zero- and one-dimensional nanostructures akin to what has been possible in the past with semiconductor heterostructures by thin film approaches. © *2007 American Institute of Physics*.
[DOI: 10.1063/1.2790496]

Fabrication and assembly of zero-dimensional (0D) and one-dimensional (1D) functional oxide nanostructures, particularly of those with magnetic and/or ferroelectric order parameters, have attracted considerable research interest in recent decades.[1–5] Properties and performance of such spatially and dimensionally constrained nanostructures are heavily influenced by the external morphology and internal microstructure. Such significant influence arises from two factors: (1) ferroelectricity and magnetism are intrinsic materials properties that are extremely sensitive to crystallinity, orientation, aspect ratio, and pattern-substrate interface structure;[6] and (2) small alterations of chemistry,[7] strain condition,[8] shape,[9] and even surface roughness[10] in low dimensional ferroic materials have a rather strong impact due to miniaturization. Therefore, it is imperative to develop innovative design strategies enabling both fabrication and engineering of the nanoscale features of functional nanopatterns.

For magnetic and ferroelectric oxides, structural and morphological control is generally achieved via "top-down" approaches in order to attain epitaxial functional devices. In these approaches, oxide thin film is first deposited with its crystalline orientation dictated by the crystallography of the substrate. The film is then patterned and etched to obtain features with defined size, shape, and separation. An inherent drawback of this two-step approach is that etching introduces critical structural flaws which pose severe problems for patterns at sub-100-nm length scale.[11,12] Furthermore, because most oxides are refractory and chemically inert, the time required for chemical etching can be prolonged.[13] Therefore, it is highly desirable to develop an etch-free route that allows for high resolution patterning as well as convenient structural and morphological control of the as-fabricated nanostructures.

We have recently introduced the "soft" electron beam lithography ("soft-*e*BL") as a site-specific fabrication approach for patterning diverse oxide nanostructures without etching process.[14] We have shown that soft-eBL enables structural engineering of oxide patterns by changing pattern dimension.[15,16] In this letter, a direct control of the morphology of epitaxial 0D and 1D oxide nanopatterns by simple tuning of *e*BL parameters is demonstrated. In particular, we show fabrication of frustum or pyramid shaped ferroelectric $BaTiO_3$ (BTO) 0D nanopatterns by changing the *e*BL resist thickness, and magnetic $CoFe_2O_4$ (CFO) in-plane single crystal nanolines with zig-zag or very smooth edges by controlling the line patterning direction with respect to underlying substrate crystallography. Using BTO nanopattern as an example, the chemical constituent distribution and the functionality of the nanostructures are investigated using analytical transmission electron microscope and piezoresponse force microscope (PFM).

The scheme of soft-*e*BL is shown in the supplementary material. The key steps include (1) development of trench pattern in *e*BL resist, (2) functionalization of inside surfaces of trenches with self-assembled monolayer and/or plasma treatment to control hydrophobicity/hydrophilicity, (3) filling the trenches with sol precursor by spinning the sol onto the patterned resist, (4) drying and lift-off to remove resist, and (5) annealing the patterned substrate to convert the as-prepared amorphous patterns into crystalline. In this study,

[a)]Electronic mail: v-dravid@northwestern.edu

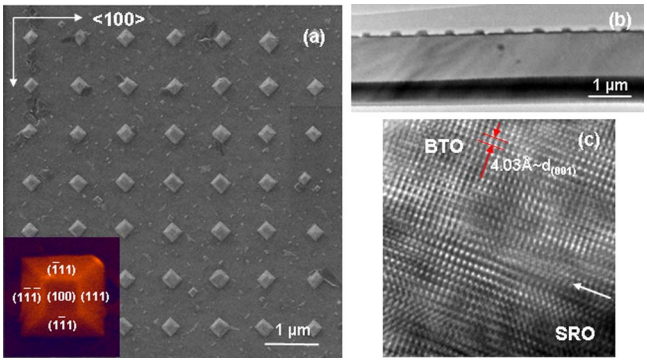

FIG. 1. (Color online) (a) ESEM image of BTO nanofrustums on (100) SRO/STO substrate. White arrows indicate the ⟨001⟩ directions of the substrate. Inset shows the possible facets of the BTO frustums. (b) TEM cross-sectional image of BTO/SRO/STO structures. Sample is cut along ⟨110⟩ direction of the substrate, through 10 nanopatterns. (c) TEM high resolution image at BTO/SRO interface showing the heteroepitaxy between the nanostructure and the substrate. Arrow indicates the interface position. The uneven background is due to the ion beam damage introduced during FIB lift-off procedure.

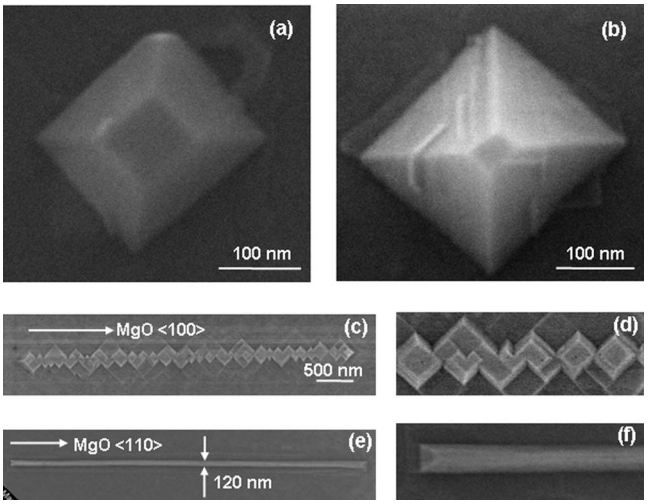

FIG. 2. [(a) and (b)] BTO frustum and pyramid, obtained by patterning with different *e*BL resist thickness. (c) ESEM image of CFO line patterned along ⟨100⟩ MgO. (d) shows detail of the zig-zag edge. (e) ESEM image of CFO line patterned along ⟨110⟩ MgO. (f) Image of one end of the line showing the faceting detail.

BTO dots were patterned on (100) $SrRuO_3$-coated $SrTiO_3$ substrate (SRO/STO), whereas CFO lines were patterned on single crystal (100) MgO substrate for epitaxy. Details on preparation of sol precursors and annealing condition are provided in supplementary material. Both *e*BL patterning and imaging of the final nanostructures were carried out in a Quanta 600F environmental scanning electron microscope (ESEM, FEI Corporation, MA). By introducing a low pressure of water vapor into the chamber, ESEM effectively eliminates surface charging on insulating materials and, therefore, allows highly precise *e*BL processing and imaging of the nanopatterns in pristine condition.[17]

Annealed BTO 0D patterns on SRO/STO are shown in Fig. 1, with 200 nm nominal width. It is interesting to note the development of frustum shape of the nanodots from the original column-shaped trenches (with 300 nm diameter) defined in *e*BL resist. From atomic force microscope (AFM) measurements (not shown here), we observed about 70% volume shrinkage of typical dot patterns after annealing due to elimination of organic component and phase transformation. The annealed BTO patterns exhibit uniform shape and well-defined facets, with four bottom edges aligned along the ⟨110⟩ directions of the substrate. Given the similar structure and close lattice parameters of BTO and SRO, this morphology suggests that the BTO frustums are single crystalline, with cube-on-cube epitaxy with respect to the substrate, as illustrated in the inset of Fig. 1(a). It is further confirmed by transmission electron microscopy (TEM) electron diffraction and high resolution imaging of the BTO/SRO interface [Fig. 1(c)]. This suggests a uniform "*a*"-domain or "*c*"-domain configuration of all BTO nanostructures, which is highly favorable to harness the ferroelectric properties of nanopatterns towards possible application such as high density memories.

The frustum edges are essentially the intercepts of side facets and the bottom surface. In the BTO/SRO case, the bottom surface is determined by the orientation of the substrate (i.e., {100}), whereas the side facets develop as {111} planes, most probably due to their low free surface energy. Therefore, the morphology development of the BTO 0D nanopatterns during annealing can be considered as the result of minimizing total surface energy of the system (including the interface between the pattern and the substrate, and the free surface energy), coupled with interfacial strain energy. The above argument has two interesting implications. First, providing enough BTO material at each patterned site, one may expect the ultimate shape of BTO pattern on SRO to be a pyramid with four {111} side planes intersecting at the top corner, in order to minimize the total surface energy. Given that *a* and *c* lattice constants for tetragonal phase BTO are very close, the aspect ratio (i.e., height/bottom width) of such pyramidal pattern is equal to the ratio between the *d* spacing of (001) plane and that of (110) plane, which is close to $1/\sqrt{2}$. That is, a pyramid with 200 nm bottom width should have a height of about 141 nm. This can be achieved by increasing the thickness of the *e*BL resist, which allows more sol precursor to be filled in each patterned trench. Second, the morphology control strategy for 0D nanostructures can be expanded to fabrication of 1D nanostructures and using other material systems that show surface energy anisotropy. This can be readily carried out in soft-*e*BL, given that it is highly material and substrate general.

We now demonstrate the shape manipulation based on the above argument. Shown in Figs. 2(a) and 2(b) is the development of a pyramid versus a frustum shaped BTO nanostructures on SRO (both with 200 nm bottom width), obtained by patterning with 600-nm-thick and 300-nm-thick resist films, respectively. The AFM analysis (not shown) reveals a 50 nm height for the frustum and a 136 nm height for the pyramid, consistent with the expected 141 nm as calculated above. In order to verify the morphology development for 1D nanostructures of materials with surface anisotropy, CFO lines are patterned on (100) MgO substrate. The CFO/(100)MgO system is an ideal example for this purpose, because surface energy of {111} is seven times smaller than that of {100} for spinel-structured CFO.[18] Figures 2(c)–2(f) are ESEM images of 4 μm long CFO lines on (100) MgO substrate. When patterned along $\langle 100\rangle_{MgO}$, the line develops into a saw-tooth-edged morphology. However, when patterned along $\langle 100\rangle_{MgO}$, the CFO line shows very flat and smooth edges. It has been reported in both micromagnetic simulations and experimental results that edge roughness of elongated magnetic nanostructures may contribute to increased

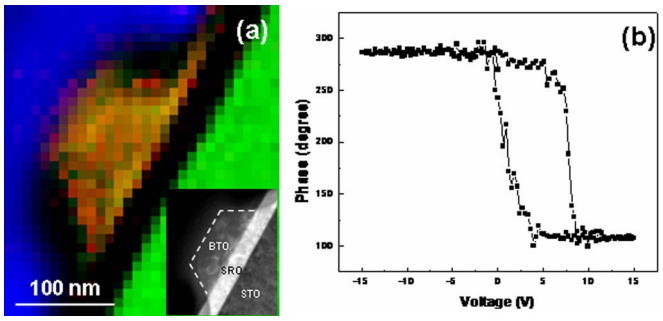

FIG. 3. (Color online) (a) EELS map across one BTO pattern showing the chemical constituent distribution. The color scheme is set as follows: green=Ti ($L_{2,3}$ edges), red=Ba ($M_{4,5}$ edges), blue=C (K edge; carbon is introduced during TEM sample preparation), which brings a yellowish hue to the BTO pattern. The black layer under BTO pattern corresponds to the SRO film. Inset shows the corresponding dark field STEM image of the pattern. Pattern edge is indicated by the dash line. (b) Bias-phase hysteresis loop obtained with PFM from one BTO nanofrustum with 200 nm width on SRO/STO substrate.

coercivity due to the edge morphology induced spin-state distortions.[10,19] Thus, the control strategy of edge morphology for magnetic oxide introduced in this letter may provide an interesting test bed to study such phenomena. Another attribute of this approach is the simplicity of shape control, i.e., dramatic morphology control of 0D or 1D nanostructures can be achieved by simply tuning the patterning parameters. This unique capability of soft-eBL to obtain "patterning-controlled morphology" implies an additional degree of freedom for the design and fabrication of oxide nanostructures for functional devices.

For BTO 0D nanopatterns, it is essential to investigate the nature of the ferroelectric-electrode interface (i.e., BTO/SRO), which is expected to have a significant effect on interfacial strain and the ferroelectric properties in sub-100-nm-thick structures.[20] The chemical constituent distribution of BTO nanofrustums at the interface was analyzed using electron energy loss spectroscopy (EELS) under the scanning transmission electron microscope (STEM) in the annular dark field mode. Figure 3(a) shows the elemental map constructed using EELS spectrum imaging with Ba ($M_{4,5}$), Ti ($L_{2,3}$), and C (K) edges. It clearly identifies the constituent elements of the nanostructure and does not imply any noticeable diffusion of Ba or Ti into SRO, even after high temperature annealing. Piezoelectric behavior of BTO 0D nanopatterns is confirmed with PFM equipped with a signal access module and an external lock-in amplifier. Figure 3(b) is a phase-bias hysteresis loop obtained from one BTO frustum. The 180° phase change with dc bias changing from negative to positive clearly verifies the piezoelectric behavior. An overall shift of the hysteresis loop toward the positive bias is observed, which may be attributed to the polarization pinning due to either mechanical stress or trapped electronic charges near the interface. Detailed investigation is under way to analyze how the size and shape of nanostructures influence the strain distribution and, therefore, the piezoelectric behavior.

In summary, a facile strategy for morphologic control of magnetic and ferroelectric 0D and 1D nanostructures, based on soft-eBL patterning technique, is demonstrated. This approach allows for direct control of crystal orientation, shape development, and edge definition during fabrication, by simply adjusting the patterning parameters such as resist thickness and pattern directions with respect to underlying substrate. This etch-free process was applied to fabricate $BaTiO_3$ pyramids, frustums, and $CoFe_2O_4$ single crystal nanolines. The structure, chemical nature, and functionality identity of the soft-eBL fabricated nanostructures were probed with a complementary set of characterization tools. Given its material and substrate generality, the proposed strategy to control the morphology of nanostructures via patterning is expected to be applicable to a wide variety of materials systems, including nonoxide systems, and may pave the way for innovative applications which require nanopatterned architecture.

The authors thank Dr. J. M. Hiller of Electron Microscopy Center, Argonne National Laboratory for help in preparing TEM sample with FIB lift-off technique, and Dr. O. Auciello of Materials Science Division, Argonne National Laboratory for help in $SrRuO_3$ deposition. This work was supported by the NSF-NSEC (Award No. EEC-0647560), NSF-MRSEC (DMR No. 0520513), and the U.S. Department of Energy (DOE-BES). The research work was performed in the EPIC and NIFTI facilities of the NU*ANCE* Center at Northwestern University. NU*ANCE* Center is supported by NSF-NSEC, NSF-MRSEC, the State of Illinois, and Northwestern University.

[1] Z. W. Pan, Z. R. Dai, and Z. L. Wang, Science **291**, 1947 (2001).
[2] M. Alexe and D. Hesse, J. Mater. Sci. **41**, 1 (2006).
[3] H. X. Fu and L. Bellaiche, Phys. Rev. Lett. **91**, 257601 (2003).
[4] H. J. Shin, J. H. Choi, H. J. Yang, Y. D. Park, Y. Kuk, and C. J. Kang, Appl. Phys. Lett. **87**, 113114 (2005).
[5] D. Ruzmetov, Y. Seo, L. J. Belenky, D.-M. Kim, X. Ke, H. Sun, V. Chandrasehar, C.-B. Eom, M. S. Rzchowaki, and X. Pan, Adv. Mater. (Weinheim, Ger.) **17**, 2869 (2005).
[6] V. Vaithyanathan, J. Lettieri, W. Tian, A. Sharan, A. Vasudevarao, Y. L. Li, A. Kochhar, H. Ma, J. Levy, P. Zschack, J. C. Woicik, L. Q. Chen, V. Gopalan, and D. G. Schlom, J. Appl. Phys. **100**, 024108 (2006).
[7] V. A. L. Roy, A. B. Djurisic, H. Liu, X. X. Zhang, Y. H. Leung, M. H. Xie, J. Gao, H. F. Lui, and C. Surya, Appl. Phys. Lett. **84**, 756 (2004).
[8] K. J. Choi, M. Biegalski, Y. L. Li, A. Sharan, J. Schubert, R. Uecker, P. Reiche, Y. B. Chen, X. Q. Pan, V. Gopalan, L. Q. Chen, D. G. Schlom, and C. B. Eom, Science **306**, 1005 (2004).
[9] Y. N. Xia, P. D. Yang, Y. G. Sun, Y. Y. Wu, B. Mayers, B. Gates, Y. D. Yin, F. Kim, and Y. Q. Yan, Adv. Mater. (Weinheim, Ger.) **15**, 353 (2003).
[10] M. T. Bryan, D. Atkinson, and R. P. Cowburn, J. Phys.: Conf. Ser. **17**, 40 (2005).
[11] A. Cofer, P. Rajora, S. DeOrnellas, and D. Keil, Integr. Ferroelectr. **16**, 53 (1997).
[12] M. Hiratani, C. Okazaki, H. Hasegawa, N. Sugii, Y. Tarutani, and K. Takagi, Jpn. J. Appl. Phys., Part 1 **36**, 5219 (1997).
[13] I. O. Owate and R. Freer, J. Am. Ceram. Soc. **75**, 1266 (1992).
[14] S. Donthu, Z. X. Pan, B. Myers, G. Shekhawat, N. G. Wu, and V. Dravid, Nano Lett. **5**, 1710 (2005).
[15] S. Donthu, T. Sun, and V. Dravid, Adv. Mater. (Weinheim, Ger.) **19**, 125 (2007).
[16] Z. X. Pan, N. Alem, T. Sun, and V. P. Dravid, Nano Lett. **6**, 2344 (2006).
[17] B. D. Myers and V. P. Dravid, Nano Lett. **6**, 963 (2006).
[18] H. Zheng, Q. Zhan, F. Zavaliche, M. Sherburne, F. Straub, M. P. Cruz, L. Q. Chen, U. Dahmen, and R. Ramesh, Nano Lett. **6**, 1401 (2006).
[19] J. G. Deak and R. H. Koch, J. Magn. Magn. Mater. **213**, 25 (2000).
[20] V. Nagarajan, C. S. Ganpule, A. Stanishevsky, B. T. Liu, and R. Ramesh, Microsc. Microanal. **8**, 333 (2002).